

Anisotropic superconducting gap probed by ^{125}Te NMR in noncentrosymmetric Sc_6MTe_2 ($M = \text{Fe}, \text{Co}$)

Kanako Doi,¹ Hayase Takei,¹ Yusaku Shinoda,² Yoshihiko Okamoto,³ Daigorou Hirai,²
Koshi Takenaka,² Taku Matsushita,¹ Yoshiaki Kobayashi,¹ and Yasuhiro Shimizu^{1,4}

¹*Department of Physics, Nagoya University, Chikusa, Nagoya 464-8602, Japan.*

²*Department of Applied Physics, Nagoya University, Chikusa, Nagoya 464-8603, Japan.*

³*Institute for Solid State Physics, University of Tokyo, Kashiwa, 277-8581, Japan.*

⁴*Department of Physics, Shizuoka University, Suruga, Shizuoka 422-8529, Japan.*

(Dated: June 12, 2025)

The superconducting gap symmetry is investigated by ^{125}Te NMR measurements on Sc_6MTe_2 ($M = \text{Fe}, \text{Co}$) without spatial inversion symmetry. The spin susceptibility obtained from the Knight shift K is suppressed below the superconducting transition temperature, while leaving a finite value down to the lowest temperature ($\simeq 0.4$ K). The nuclear spin-lattice relaxation rate $1/T_1$ follows a power law against temperature T without showing a coherence peak characteristic of the isotropic gap. The result implies a pairing admixture or a residual density of states under magnetic field. The normal metallic state has a Korringa scaling relation between $1/T_1T$ and the Knight shift, reflecting a weak electron correlation.

I. INTRODUCTION

Noncentrosymmetric superconductors have attracted attention due to parity mixing and reciprocal transport [1–5]. The antisymmetric spin-orbit coupling under strong spin-orbit coupling and broken spatial inversion brings out unconventional Cooper pairing with a mixed parity of even spin-singlet and odd spin-triplet symmetry [6]. Topological superconductors including a spin-triplet superconductor with Majorana bound states provide a significant platform for topological quantum computation that implements error corrections against local perturbation [7]. The hallmark experimental evidence for spin-triplet pairing satisfies anisotropic spin susceptibility, enhanced Pauli-limiting field, zero-bias conductance, and time-reversal symmetry breaking [8–10]. Noncentrosymmetric superconductors have been studied extensively in rare-earth metals such as CePt_3Si [6, 11–13], transition-metal alloys [14–19], topological semimetals [20], and artificial superlattice [21]. The parity admixture strongly depends on electron correlation and spin-orbit coupling [9]. Thus, a physical and chemical tuning of these parameters is desired to quantitatively uncover the effect of antisymmetric spin-orbit coupling on superconducting pairing symmetry.

Ternary scandium tellurides Sc_6MTe_2 (M : transition metals) have a hexagonal Zr_6CoAl_2 -type structure without inversion symmetry [22, 23]. Superconductivity was discovered in Sc_6FeTe_2 with a hexagonal $P6_2m$ (D_{3h}^3 , No.189) lattice at the highest transition temperature $T_c = 4.7$ K among a series of materials [24]. The upper critical field extrapolated to 0 K reaches 8.7 T, which is comparable to the Pauli paramagnetic limit. The second highest $T_c = 3.6$ K has been observed in Sc_6CoTe_2 having the same lattice symmetry [24]. Although the band splitting due to spin-orbit coupling and inversion symmetry breaking is smaller than that of rare-earth compounds, the strength of the electron correlation can be system-

atically tuned by a chemical substitution of the M site with $3d$, $4d$, and $5d$ transition metals. The density of states $D(E_F)$ at the Fermi level E_F is mainly composed of Sc and M bands in the band calculation. E_F is located close to a peak of $D(E)$ for $M = \text{Fe}$ and a valley for Co. The Sommerfeld coefficient obtained from the specific heat, $\gamma = 73$ (Fe) and 55 (Co) mJ/K²mol, is significantly greater than the calculated free electron value $\gamma \sim 22$ mJ/K²mol, suggesting a strong electron correlation. The specific heat jump ($\Delta C/\gamma T_c = 2.4$) in Sc_6FeTe_2 at T_c well exceeds the value ($\Delta C/\gamma T_c = 1.43$) expected for the weak-coupling Bardeen-Cooper-Schrieffer (BCS) superconductor and thus implies strong-coupling superconductivity.

We utilize NMR spectroscopy as a powerful probe of parity mixing in noncentrosymmetric superconductors with strong spin-orbit coupling [25–34]. The Knight shift, which measures the local spin susceptibility at the selected atomic site, distinguishes the predominant contribution from the spin-singlet and spin-triplet pairing. Since spin is not the conservative quantity under spin-orbit coupling, the possibility of the spin-triplet admixture state must be carefully examined from the pseudo-spin susceptibility [35]. The nuclear spin-lattice relaxation rate $1/T_1$ as a function of temperature measures the coherence factor of superconducting pairing and thus measures the spatial symmetry of the order parameter.

In this paper, we investigate the local spin susceptibility of superconducting and normal states through ^{125}Te NMR measurements on Sc_6FeTe_2 and Sc_6CoTe_2 without inversion symmetry. The NMR spectrum uncovers the absence or presence of the structural symmetry-breaking transition. The results of Knight shift and $1/T_1T$ are compared with the first-principles band calculation. We examine the possible pairing symmetry and the effect of electron correlation.

II. EXPERIMENTAL

^{125}Te NMR measurements were conducted on polycrystalline samples of Sc_6MTe_2 ($M = \text{Fe}, \text{Co}$) synthesized with the arc melting method under Ar atmosphere [22–24]. The sample was dispersed in melted paraffin to avoid eddy current under NMR radio frequency (rf) pulses. Instead of the ^{45}Sc nuclear spin ($^{45}I = 7/2$) with a complex quadrupole-split NMR spectrum, here we performed ^{125}Te ($^{125}I = 1/2$) NMR with a simple spectrum. T_c under magnetic field was determined from a diamagnetic response of the *in situ* tank circuit and the intensity of the NMR signal. The NMR spectrum was measured under static magnetic fields of 2.57 and 9.13 T in the superconducting and normal states, respectively. The NMR spectrum was obtained from the Fourier transformation of the spin-echo signal taken after the rf pulses with the interval time $\tau = 30 \mu\text{s}$ and the duration $t_{\pi/2} = 2 \mu\text{s}$. ^{125}Te Knight shift defined by $K = (\omega - \omega_0)/\omega_0$ from the resonance frequency ω using the reference frequency $\omega_0 = \gamma_n H$, where the bare gyromagnetic ratio $\gamma_n/2\pi = 13.454 \text{ MHz/T}$. The rf power dependence of the Knight shift was measured at 1.4 K, keeping the pulse length constant. We find no power dependence between 100 and 6 mJ, which provides evidence for the negligible heating effect below T_c . $1/T_1$ was measured with a saturation recovery method in which the nuclear magnetization recovery follows a single-exponential function above T_c and becomes a stretched exponential with exponent $\beta = 0.8\text{--}1$ below T_c .

III. EXPERIMENTAL RESULTS AND DISCUSSION

A single ^{125}Te NMR spectrum was observed at high temperatures, as shown in Fig. 1, consistent with the single Te site of the $P\bar{6}2m$ lattice. The nearly symmetric spectrum reflects the isotropic hyperfine coupling tensor and spin susceptibility. The spectrum of Sc_6FeTe_2 shifts to a lower frequency and broadens upon cooling. The line shape becomes asymmetric at low temperatures, which implies a distribution of the local spin susceptibility or an inhomogeneous dipole field from magnetic impurities.

The Knight shift K determined from the peak position scales to χ below 200 K, as shown in Fig. 2(a). As the bulk spin susceptibility χ increases upon cooling (a solid curve on the right-hand axis), the negative Knight shift represents the negative hyperfine coupling constant due to the predominant core polarization of *s*-electron spins. The linearity of the $K - \chi$ plot yields the hyperfine coupling constant $H_{\text{hf}} = -0.8(2) \text{ T}/\mu_B$ for Sc_6FeTe_2 . The detail of the $K - \chi$ analysis is described in the Appendix A.

For Sc_6CoTe_2 , the ^{125}Te NMR spectrum is also narrow at high temperatures, as shown in Fig. 1. In contrast to Sc_6FeTe_2 , the spectrum starts to broaden around $T^* \sim 150 \text{ K}$ and splits into two at lower temperatures. The

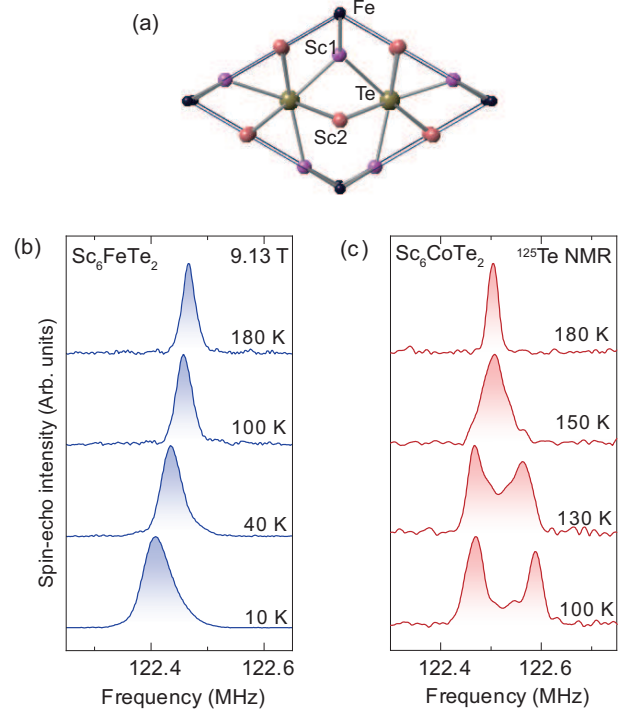


FIG. 1. (a) Crystal structure of Sc_6FeTe_2 . Temperature dependence of ^{125}Te NMR spectrum for (b) Sc_6FeTe_2 and (c) Sc_6CoTe_2 under magnetic field $H_0 = 9.13 \text{ T}$.

splitting indicates a doubling of the Te site by breaking the mirror symmetry in the unit cell. The transition occurs continuously, as shown in Fig. 1(b), where K defined by each spectral peak shows the contrasting temperature dependence below T^* : one Te spectrum shifts to a higher frequency just below T^* , while another shifts to a lower side.

For $^{125}I = 1/2$ without an electric quadrupole interaction, a spectral splitting comes purely from a magnetic origin, e.g. the difference in the local density of states between two Te sites. An increase in the averaged shift of two spectra below T^* represents a suppression of χ for the negative hyperfine coupling constant. The scaling between the averaged K yields $H_{\text{hf}} = -3.4(3) \text{ T}/\mu_B$. Since the density of states at the Fermi level, $D(E_F)$, is governed by the transition metal M and the scandium sites in the band structure calculation [24], the hyperfine coupling at the Te sites would come from the transferred interaction with surrounding ions. The observed structural transition in Sc_6CoTe_2 implies a structural instability for a symmetry lowering possibly due to the orbital-lattice coupling of transition metals.

A weak thermal variation of K and spin susceptibility is attributed to the dependence of $D(E_F)$ averaged over the energy range of $k_B T$. The spin susceptibility proportional to $D(E_F)$ is enhanced (or suppressed) when E_F is located close to the ridge (or valley) of the density of states, consistent with the band calculation in Sc_6FeTe_2 .

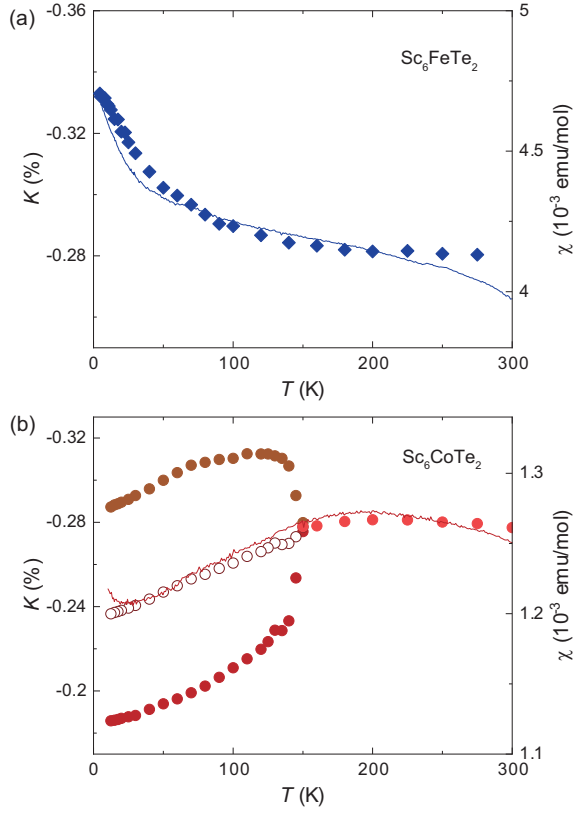


FIG. 2. ^{125}Te Knight shift K (the left-hand axis) and the bulk magnetic susceptibility χ (solid curves, the right-hand axis) against temperature T for (a) Sc_6FeTe_2 and (b) Sc_6CoTe_2 . Open symbols in (b) are the averaged K for two Te sites below T^* . Note that both vertical axes are expanded for clarity.

(Sc_6CoTe_2), respectively [24].

At low fields below H_{c2} , the Knight shift gives the spin susceptibility in the superconducting phase. We measured ^{125}Te NMR spectra across T_c at $H = 2.57$ T well below H_{c2} . T_c is obtained as 3.4 and 2.5 K for Sc_6FeTe_2 and Sc_6CoTe_2 , respectively at $H = 2.6$ T in the resistivity measurement [24]. As shown in Fig. 3, the peak frequency of the spectrum is almost independent of the temperature in the normal state below 10 K and starts to shift in a positive direction below T_c for Sc_6FeTe_2 . For a negative hyperfine coupling constant, the spin susceptibility is suppressed below T_c , as expected in spin-singlet superconductors [36].

For Sc_6CoTe_2 , one of the spectra at the lower frequency exhibits a positive shift below T_c , as shown in Fig. 3(b). In contrast, the spectrum for the higher frequency exhibits a tiny shift. The site-dependent shift rules out the extrinsic origin due to the Meissner effect and reflects the difference in the spin density between two Te sites, which participates in the superconducting pairing. For the negative hyperfine coupling, the positive Knight shift also indicates a decrease in spin susceptibility below T_c . The residual value at the lowest temperature can be attributed to the paramagnetic component arising from

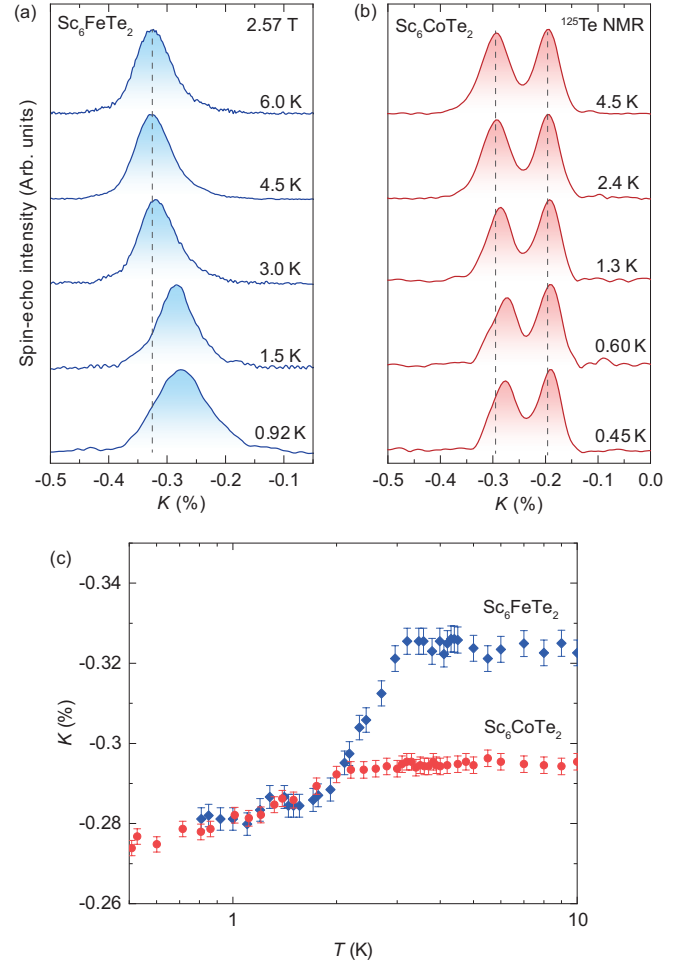


FIG. 3. Temperature dependence of ^{125}Te NMR spectra for (a) Sc_6FeTe_2 and (b) Sc_6CoTe_2 across T_c at $H_0 = 2.57$ T. Dashed lines indicate the peak positions above T_c . (c) K obtained from the peak position of the NMR spectrum. Only the lower frequency shift is plotted in Sc_6CoTe_2 .

spin-triplet pairing or a residual density of states.

The Knight shift generally consists of the spin part K_s and the orbital part K_{orb} . Assuming Korringa's relation described in the following, the orbital part K_{orb} is evaluated from the $K-(T_1T)^{-0.5}$ plot as $K_{\text{orb}} = 0.02\%$ for Sc_6FeTe_2 and $K_{\text{orb}} = 0.05\%$ for Sc_6CoTe_2 (See Appendix A). The difference of K between the normal and superconducting states is tiny: $\Delta K = 0.04\%$ for Sc_6FeTe_2 and $\Delta K = 0.02\%$ for Sc_6CoTe_2 [Fig. 3(c)], which are one order smaller than those expected in the spin-singlet state. The spectral broadening below T_c can be attributed to a magnetic impurity and the penetration of vortex cores.

The superconducting gap structure was investigated by $1/T_1$ in a magnetic field of 2.57 T, as shown in Fig. 4. $1/T_1$ linearly decreases with temperature in the normal state and shows a steep drop below $T_c = 3.3$ and 2.2 K for Sc_6FeTe_2 and Sc_6CoTe_2 , respectively. The coherence peaks expected in s -wave superconductors were not observed just below T_c . Instead, $1/T_1$ follows the power

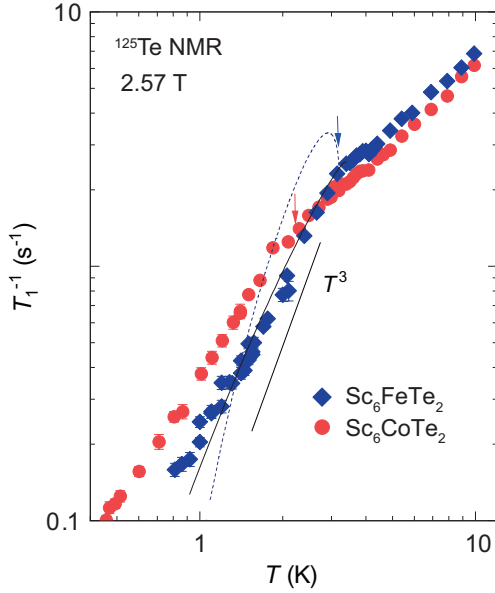


FIG. 4. Temperature dependence of $1/T_1$ measured at 2.57 T. Arrows indicate the superconducting transition temperature T_c determined by the zero resistance [24] and the *in-situ* ac susceptibility measurement. The dotted and solid curves are numerical calculations for conventional full gap [37] and line-node gap superconductor. The solid line is a guide of the power law ($\sim T^3$).

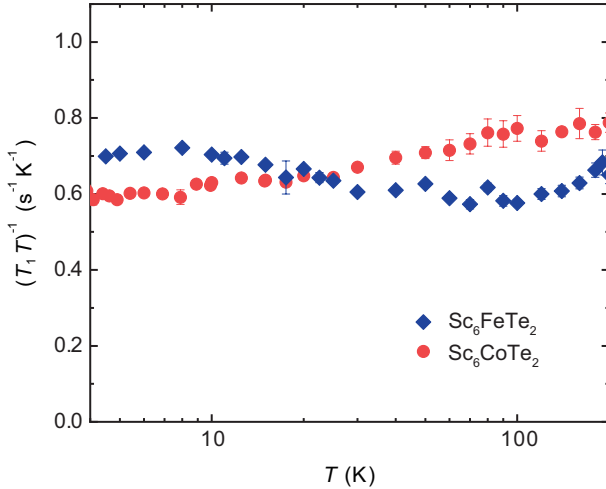


FIG. 5. Nuclear spin-lattice relaxation rate divided by temperature, $(T_1T)^{-1}$, on Sc_6FeTe_2 and Sc_6CoTe_2 at $H = 9.13$ T. We obtained T_1 for the integrated spin-echo intensity of the two Te sites in Sc_6CoTe_2 below T^* . No indication of a magnetic transition is observed at 150 K, where the NMR spectrum starts to split.

law $\propto T^n$ ($n \simeq 3$) rather than the exponential function expected in a full-gap superconductor. The result is consistent with the presence of line nodes in the quasiparticle excitation gap.

In standard metals, $1/T_1T$ is proportional to the square of $D(E_F)$. As shown in Fig. 5, $1/T_1T$ in-

creases slightly or decreases upon cooling for Sc_6FeTe_2 and Sc_6CoTe_2 , respectively. The behavior is similar to those of χ and K proportional to $D(E_F)$ in Fig. 2. Therefore, Korriga's relation, $1/T_1T \propto K_s^2$, holds in both compounds (See also the Appendix A). That is, the ratio $1/T_1TK_s^2$ takes the universal constant called the Korriga constant $\mathcal{K}_\alpha = \frac{\hbar}{4\pi k_B} \left(\frac{\gamma_e}{\gamma_n} \right)^2 \frac{1}{T_1TK_s^2}$, where γ_e is the electron gyromagnetic ratio. \mathcal{K}_α would be progressively enhanced or suppressed against temperature in the presence of antiferromagnetic or ferromagnetic fluctuations, respectively. Here we obtained temperature-independent $\mathcal{K}_\alpha = 1.0$ for Sc_6FeTe_2 and 1.3 for Sc_6CoTe_2 , suggesting a negligible effect of spin fluctuations in the normal state.

In a weakly correlated metal, the superconducting order parameter would have a *s*-wave nature, as anticipated from the BCS theory mediated by phonons, whereas it can be anisotropic in the presence of strong electron-electron and electron-phonon coupling. In Sc_6MTe_2 , superconductivity induced by strong electron-phonon coupling has been recently proposed on the basis of the *ab initio* calculation [38], where the anharmonic low-frequency phonon (rattling) mode plays a crucial role in superconductivity. Strong coupling superconductivity was also expected from the specific heat behavior across T_c in Sc_6FeTe_2 [24], which is compatible with the present NMR results showing the anisotropic order parameter. The strong electron-phonon coupling, if any, can be observed as an enhancement of $1/T_1T$, as is known in KOs_2O_6 having a rattling phonon mode [39]. To uncover the phonon dynamics, we have measured $1/T_1$ at the ^{45}Sc sites with electric quadrupole interaction for Sc_6FeTe_2 . It also follows Korriga's law without the enhancement of $1/T_1T$ in the normal metallic state.

Note that the coherence peak is sensitively suppressed in the presence of magnetic field and impurities [40–43]. The gap structure and topology can change by impurities, as discussed in Fe pnictide superconductors [44]. For Sc_6FeTe_2 , the Sommerfeld coefficient γ_0 remains finite even under zero magnetic field and increases with magnetic field, implying a small amount of extrinsic normal-state domain around defects [24]. We observed a slight suppression of the stretched exponent well below T_c , indicating the residual normal state under the magnetic field. Although further low-field experiments are desired, we have not succeeded in detecting the NMR signal of the superconducting phase at lower fields due to the Meissner shielding against the rf pulse.

In Sc_6MTe_2 , the band splitting due to the absence of the inversion symmetry would be too small to admit the spin-singlet and spin-triplet pairing [24]. If the spin-triplet component exists, the spin susceptibility depends on the magnetic field direction: it is independent of temperature in a magnetic field parallel to the *d*-vector of spin-orbit coupling, while it decreases below T_c for a field normal to the *d* vector. Taking into account the *d* vector parallel to the *c* axis, spin susceptibility would decrease along the in-plane direction, leading to a positive change

below T_c . Then, the NMR spectrum for a powder sample is distorted into the axially anisotropic powder pattern in the superconducting phase, which does not match our experimental result. For confirmation of parity mixing, it would be necessary to measure the anisotropy of the spin susceptibility on a single crystal.

IV. CONCLUSION

In conclusion, the symmetry of the superconducting order parameter was investigated on the noncentrosymmetric Sc_6MTe_2 without inversion symmetry through ^{125}Te NMR measurements. The spin susceptibility obtained from the Knight shift is suppressed below T_c , consistent with the spin-singlet pairing, while the large residual value implies parity mixing of the spin-triplet and singlet components due to spin-orbit coupling. The temperature dependence of $1/T_1$ provides evidence for the nodal gap in the quasiparticle excitation. The possibility of spin-singlet and triplet superconductivity should be carefully considered through lower-field experiments with a high-quality single crystal.

ACKNOWLEDGEMENTS

We are thankful for useful discussion with Y. Yamakawa and H. Kontani. We acknowledge support from grants-in-aid in scientific research by JSPS (No. JP19H05824, No. 22H05256, No. 22K03510, No. 23H04025, and No. 24H00954).

Appendix A: Evaluation of orbital Knight shift

As described above, the NMR Knight shift consists of spin and orbital parts. The spin part K_s can depend on temperature and be proportional to spin susceptibility. The orbital part K_{orb} governed by the Van-Vleck orbital susceptibility is independent of temperature and subtracted from the K versus χ plot in Fig. 6. Good linearity is observed in the temperature range of 100–180 K and 20–200 K for Sc_6FeTe_2 and Sc_6CoTe_2 , respectively. The linearity yields the hyperfine coupling constant, as described in the main text. The crossing points between spin and orbital linearity give the constant offset $K_{\text{orb}} = 0.29\%$ (Fe) and 0.48% (Co).

In Fermi liquid metal without spin fluctuations, K_s and $(T_1T)^{-1}$ are proportional to $D(E_F)$ and $D(E_F)^2$, respectively. Then K_s is linear to $(T_1T)^{-0.5}$ as an implicit function of temperature. Here the orbital contribution in $(T_1T)^{-1}$ would be negligible for Te sites without orbital degeneracy. The extrapolation in the $K-(T_1T)^{-0.5}$

linearity can be another way to evaluate K_{orb} [45], which should be consistent with the $K-\chi$ plot.

We find a good linear relation between K and $(T_1T)^{-0.5}$, as shown in Fig. 7. We obtained $K_{\text{orb}} =$

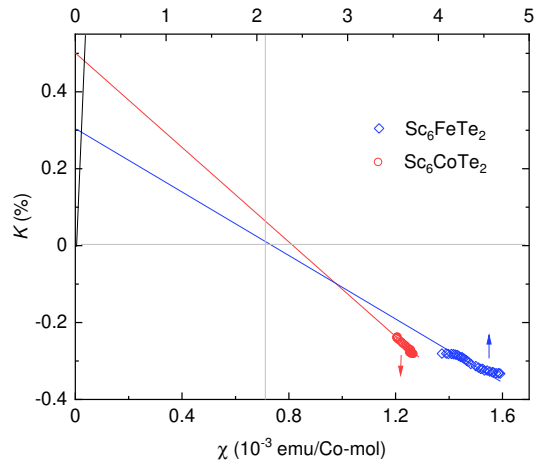


FIG. 6. Knight shift vs bulk magnetic susceptibility as an implicit function of temperature for Sc_6FeTe_2 and Sc_6CoTe_2 at $H = 9.13$ T. K was defined as an average shift for two Te sites in Sc_6CoTe_2 below T^* . The black line is the calculated orbital shift.

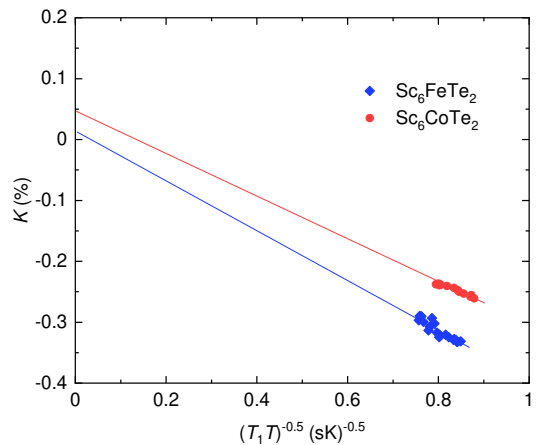


FIG. 7. Knight shift K plotted against the square of the nuclear spin-lattice relaxation rate divided by temperature, $(T_1T)^{-0.5}$, on Sc_6FeTe_2 and Sc_6CoTe_2 at $H = 9.13$ T.

0.02% and 0.05% , which is largely different from the $K-\chi$ plot. The discrepancy may come from the significant constant offset of the bulk magnetization, as observed in Fe and Co pnictide superconductors [46, 47]. In the present case, it can be attributed to the small amount of magnetic impurities.

-
- [1] E. Bauer and M. Sigrist, *Non-Centrosymmetric Superconductors: Introduction and Overview* (Springer, Berlin, 2012).
- [2] M. Smidman, M. B. Salamon, H. Q. Yuan, and D. F. Agterberg, Superconductivity and spin-orbit coupling in non-centrosymmetric materials: a review, *Rep. Prog. Phys.* **80**, 036501 (2017).
- [3] S. Yip, Noncentrosymmetric superconductors, *Ann. Rev. Condens. Mat. Phys.* **5**, 15 (2014).
- [4] R. Wakatsuki, Y. Saito, S. Hoshino, Y. M. Itahashi, T. Ideue, M. Ezawa, Y. Iwasa, and N. Nagaosa, Nonreciprocal charge transport in noncentrosymmetric superconductors, *Sci. Adv.* **3**, e1602390 (2017).
- [5] Y. Tokura and N. Nagaosa, Nonreciprocal responses from non-centrosymmetric quantum materials, *Nat. Commun.* **9**, 3740 (2018).
- [6] P. A. Frigeri, D. F. Agterberg, A. Koga, and M. Sigrist, Superconductivity without inversion symmetry: MnSi versus CePt₃Si, *Phys. Rev. Lett.* **92**, 097001 (2004).
- [7] M. Sato and S. Fujimoto, Majorana fermions and topology in superconductors, *J. Phys. Soc. Jpn.* **85**, 072001 (2016).
- [8] L. P. Gor'kov and E. I. Rashba, Superconducting 2d system with lifted spin degeneracy: mixed singlet-triplet state, *Phys. Rev. Lett.* **87**, 037004 (2001).
- [9] S. Fujimoto, Electron correlation and pairing states in superconductors without inversion symmetry, *J. Phys. Soc. Jpn.* **76**, 051008 (2007).
- [10] M. Mandal, N. C. Drucker, P. Siriviboon, T. Nguyen, A. Boonkird, T. N. Lamichhane, R. Okabe, A. Chotrat-anapituk, and M. Li, Topological superconductors from a materials perspective, *Chem. Mater.* **35**, 6184 (2023).
- [11] E. Bauer, G. Hilscher, H. Michor, C. Paul, E. W. Scheidt, A. Griбанov, Y. Seropegin, H. Noël, M. Sigrist, and P. Rogl, Heavy fermion superconductivity and magnetic order in noncentrosymmetric CePt₃Si, *Phys. Rev. Lett.* **92**, 027003 (2004).
- [12] I. Bonalde, W. Brämer-Escamilla, and E. Bauer, Evidence for line nodes in the superconducting energy gap of noncentrosymmetric CePt₃Si from magnetic penetration depth measurements, *Phys. Rev. Lett.* **94**, 207002 (2005).
- [13] K. V. Samokhin, E. S. Zijlstra, and S. K. Bose, CePt₃Si: an unconventional superconductor without inversion center, *Phys. Rev. B* **69**, 094514 (2004).
- [14] K. Togano, P. Badica, Y. Nakamori, S. Orimo, H. Takeya, and K. Hirata, Superconductivity in the metal rich Li-Pd-B ternary boride, *Phys. Rev. Lett.* **93**, 247004 (2004).
- [15] K.-W. Lee and W. E. Pickett, Crystal symmetry, electron-phonon coupling, and superconducting tendencies in Li₂Pd₃B and Li₂Pt₃B, *Phys. Rev. B* **72**, 174505 (2005).
- [16] A. D. Hillier, J. Quintanilla, and R. Cywinski, Evidence for time-reversal symmetry breaking in the noncentrosymmetric superconductor LaNiC₂, *Phys. Rev. Lett.* **102**, 117007 (2009).
- [17] J.-K. Bao, J.-Y. Liu, C.-W. Ma, Z.-H. Meng, Z.-T. Tang, Y.-L. Sun, H.-F. Zhai, H. Jiang, H. Bai, C.-M. Feng, Z.-A. Xu, and G.-H. Cao, Superconductivity in quasi-one-dimensional K₂Cr₃As₃ with significant electron correlations, *Phys. Rev. X* **5**, 011013 (2015).
- [18] J. A. T. Barker, D. Singh, A. Thamizhavel, A. D. Hillier, M. R. Lees, G. Balakrishnan, D. M. Paul, and R. P. Singh, Unconventional superconductivity in La₇Ir₃ revealed by muon spin relaxation, *Phys. Rev. Lett.* **115**, 267001 (2015).
- [19] T. Shang, M. Smidman, A. Wang, L.-J. Chang, C. Baines, M. K. Lee, Z. Y. Nie, G. M. Pang, W. Xie, W. B. Jiang, M. Shi, M. Medarde, T. Shiroka, and H. Q. Yuan, Simultaneous nodal superconductivity and time-reversal symmetry breaking in the noncentrosymmetric superconductor CaPtAs, *Phys. Rev. Lett.* **124**, 207001 (2020).
- [20] M. N. Ali, Q. D. Gibson, T. Klimczuk, and R. J. Cava, Noncentrosymmetric superconductor with a bulk three-dimensional dirac cone gapped by strong spin-orbit coupling, *Phys. Rev. B* **89**, 020505 (2014).
- [21] F. Ando, Y. Miyasaka, T. Li, J. Ishizuka, T. Arakawa, Y. Shiota, T. Moriyama, Y. Yanase, and T. Ono, Observation of superconducting diode effect, *Nature (London)* **584**, 373 (2020).
- [22] L. Chen and J. D. Corbett, New variants of the Fe₂P structure type Sc₆TTe₂, *Inorg. Chem.* **43**, 436 (2004).
- [23] P. A. Maggard and J. D. Corbett, Sc₆mTe₂ ($m = \text{Mn, Fe, Co, Ni}$): members of the flexible Zr₆CoAl₂-type family of compounds, *Inorg. Chem.* **39**, 4143 (2000).
- [24] Y. Shinoda, Y. Okamoto, Y. Yamakawa, H. Matsumoto, D. Hirai, and K. Takenaka, Superconductivity in ternary scandium telluride Sc₆MTe₂ with 3d, 4d, and 5d transition metals, *J. Phys. Soc. Jpn.* **92**, 103701 (2023).
- [25] N. Hayashi, K. Wakabayashi, P. A. Frigeri, and M. Sigrist, Nuclear magnetic relaxation rate in a noncentrosymmetric superconductor, *Phys. Rev. B* **73**, 092508 (2006).
- [26] M. Nishiyama, Y. Inada, and G.-q. Zheng, Superconductivity of the ternary boride Li₂Pd₃B probed by ¹¹B NMR, *Phys. Rev. B* **71**, 220505 (2005).
- [27] M. Nishiyama, Y. Inada, and G.-q. Zheng, Spin triplet superconducting state due to broken inversion symmetry in Li₂Pt₃B, *Phys. Rev. Lett.* **98**, 047002 (2007).
- [28] Y. Yanase and M. Sigrist, Superconductivity and magnetism in non-centrosymmetric system: Application to CePt₃Si, *J. Phys. Soc. Jpn.* **77**, 124711 (2008).
- [29] H. Mukuda, T. Fujii, T. Ohara, A. Harada, M. Yashima, Y. Kitaoka, Y. Okuda, R. Settai, and Y. Onuki, Enhancement of superconducting transition temperature due to the strong antiferromagnetic spin fluctuations in the noncentrosymmetric heavy-fermion superconductor CeIrSi₃: A ²⁹Si NMR study under pressure, *Phys. Rev. Lett.* **100**, 107003 (2008).
- [30] M. Kandatsu, M. Nishiyama, Y. Inada, and G.-q. Zheng, Nuclear spin-lattice relaxation in non-centrosymmetric superconductors Li₂(Pd,Pt)₃B, *J. Phys. Soc. Jpn.* **77**, 348 (2008).
- [31] K. Matano, S. Maeda, H. Sawaoka, Y. Muro, T. Takabatake, B. Joshi, S. Ramakrishnan, K. Kawashima, J. Akimitsu, and G.-q. Zheng, NMR and NQR studies on non-centrosymmetric superconductors Re₇B₃, LaBiPt, and BiPd, *J. Phys. Soc. Jpn.* **82**, 084711 (2013).
- [32] K. Matano, K. Arima, S. Maeda, Y. Nishikubo, K. Kudo, M. Nohara, and G.-q. Zheng, Spin-singlet superconductivity with a full gap in locally noncentrosymmetric SrP-

- tAs, Phys. Rev. B **89**, 140504 (2014).
- [33] Y. Nagase, M. Manago, J. Hayashi, K. Takeda, H. Tou, E. Matsuoka, H. Sugawara, H. Harima, and H. Kotegawa, Observation of multigap and coherence peak in the non-centrosymmetric superconductor CaPtAs: ^{75}As nuclear quadrupole resonance measurements, Phys. Rev. B **107**, 104512 (2023).
 - [34] M. Yogi, Y. Kitaoka, S. Hashimoto, T. Yasuda, R. Settai, T. D. Matsuda, Y. Haga, Y. Ōnuki, P. Rogl, and E. Bauer, Evidence for a novel state of superconductivity in noncentrosymmetric CePt₃Si: a ^{195}Pt -NMR study, Phys. Rev. Lett. **93**, 027003 (2004).
 - [35] P. A. Frigeri, D. F. Agterberg, and M. Sigrist, Spin susceptibility in superconductors without inversion symmetry, New J. Phys. **6**, 115 (2004).
 - [36] K. Yosida, Paramagnetic susceptibility in superconductors, Phys. Rev. **110**, 769 (1958).
 - [37] L. C. Hebel and C. P. Slichter, Nuclear relaxation in superconducting aluminum, Phys. Rev. **107**, 901 (1957).
 - [38] M.-C. Jiang, R. Masuki, G.-Y. Guo, and R. Arita, Ab initio study on magnetism suppression, anharmonicity, rattling mode, and superconductivity in Sc₆MTe₂ ($M=\text{Fe}, \text{Co}, \text{Ni}$), Phys. Rev. B **110**, 104505 (2024).
 - [39] M. Yoshida, K. Arai, R. Kaido, M. Takigawa, S. Yonezawa, Y. Muraoka, and Z. Hiroi, NMR observation of rattling phonons in the pyrochlore superconductor KOs₂O₆, Phys. Rev. Lett. **98**, 197002 (2007).
 - [40] Y. Masuda and M. Hashimoto, Nmr studies on magnetic impurity effect in type II superconductors, J. Phys. Soc. Jpn. **31**, 1661 (1971).
 - [41] H.-Y. Choi and E. J. Mele, Effects of impurity vertex correction on the nmr coherence peak in s-wave superconductors, Phys. Rev. B **52**, 7549 (1995).
 - [42] B. Mitrović and K. V. Samokhin, Effect of disorder on the NMR relaxation rate in two-band superconductors, Phys. Rev. B **74**, 144510 (2006).
 - [43] J. Yang, Z. T. Tang, G. H. Cao, and G.-q. Zheng, Ferromagnetic spin fluctuation and unconventional superconductivity in Rb₂Cr₃As₃ revealed by ^{75}As NMR and NQR, Phys. Rev. Lett. **115**, 147002 (2015).
 - [44] Y. Mizukami, M. Konczykowski, Y. Kawamoto, S. Kurata, S. Kasahara, K. Hashimoto, V. Mishra, A. Kreisel, Y. Wang, P. J. Hirschfeld, Y. Matsuda, and T. Shibauchi, Disorder-induced topological change of the superconducting gap structure in iron pnictides, Nat. Commun. **5**, 5657 (2014).
 - [45] S. Harada, J. J. Zhou, Y. G. Yao, Y. Inada, and G.-q. Zheng, Abrupt enhancement of noncentrosymmetry and appearance of a spin-triplet superconducting state in Li₂(Pd_{1-x}Pt_x)₃B beyond $x = 0.8$, Phys. Rev. B **86**, 220502 (2012).
 - [46] K. Ahilan, T. Imai, A. S. Sefat, and F. L. Ning, Nmr investigation of spin correlations in BaCo₂As₂, Phys. Rev. B **90**, 014520 (2014).
 - [47] J. Cui, B. Roy, M. A. Tanatar, S. Ran, S. L. Bud'ko, R. Prozorov, P. C. Canfield, and Y. Furukawa, Antiferromagnetic spin correlations and pseudogaplike behavior in Ca(Fe_{1-x}Co_x)₂As₂ studied by ^{75}As nuclear magnetic resonance and anisotropic resistivity, Phys. Rev. B **92**, 184504 (2015).